Int. J. Electrochem. Sci., 7 **(2012)** 1937 - 1945

International Journal of ELECTROCHEMICAL SCIENCE
www.electrochemsci.org

The Mechanism of Carrier Transportation in a Superlattice Infrared Photodetector Sandwiched by Front and Rear Barriers

Shih-Hung Lin[1], *David Jui-Yang Feng*[2], *Ming-Lun Lee*[1], *Jen-Hsiang Lu*[1], *Tai-Ping Sun*[3], *Tsong-Sheng Lay*[4], *Chieh-Hsiung Kuan*[1,*]

[1] Department of Electrical Engineering and Graduate Institute of Electronics Engineering, National Taiwan University, Taipei 10617, Taiwan,
[2] Department of Electrical Engineering, National University of Kaohsiung, Kaohsiung 804, Taiwan,
[3] Department of Electrical Engineering, National Chi-Nan University, Puli 545, Taiwan,
[4] Department of Photonics and Institute of Electro-Optical Engineering, National Sun Yat-Sen University, Kaohsiung 804, Taiwan
[*]E-mail: kuan@cc.ee.ntu.edu.tw

Received: 4 July 2011 / *Accepted:* 20 January 2012 / *Published:* 1 March 2012

Photocurrent enhancement of superlattice infrared photodetector (SLIP) is demonstrated using SL sandwiched between front (thin) and rear (thick) barriers. These two barriers are utilized for photo-excited electrons in second miniband oscillate between them and punch through the front barrier to enhance tunneling probability. However, the supply of electrons is limited by the thick barrier and thus we need to fabricate the emitter contact on the SL. The experimental results of this SLIP shows higher responsivity at low bias (0.15 V, 0.20 V and 0.25 V) and one-order higher associated detectivity (1.2×10^{10} cmHz$^{1/2}$/W, at 80 K) than conventional single-barrier SLIP. Due to better performance at low bias, this SLIP is suitable for low power consumption applications.

Keywords: Superlattice, Infrared photodetector, miniband,

1. INTRODUCTION

In recent years, quantum-well infrared photodetectors (QWIPs) have attracted more and more attention such as civil, military, and medical applications. The QWIP-based focal plane array (FPA) system with high performance has been demonstrated because of the highly developed epitaxy growth and process technology [1-5]. Superlattice (SL) is also a promising fundamental structure to fabricate infrared detector. In general, the structure of an ordinary SLIP is period of superlattice integrated with

a single barrier. The roles of the single barrier are to reduce the dark current and act as a bias-tuned energy filter. [6, 7].

Because bias dropped only on the single barrier, low-bias operation is needed for SLIP. Therefore it can achieve aims of the low dark current and low power consumption. Since there is no electric field across the SL, the electron mobility in SL is relatively low. On the other hand, photoelectrons can move back or forth in the second miniband of SL and only the forward electrons can punch through the thin barrier contribute to the photocurrent. Some backward and escaping photo-electrons have no contribution to photocurrent. Due to these factors, the responsivity of SLIPs is much lower than that of the QWIPs.

In this paper, we design and study a SLIP whose structure is a 15-period SL sandwiched between front and rear barriers. The two barriers with different thickness are used for the photoelectrons to oscillate inside the SL to increase the probability of electrons emitting toward the collector, and thus more photoelectrons inject through the thin barrier to generate the higher photocurrent.

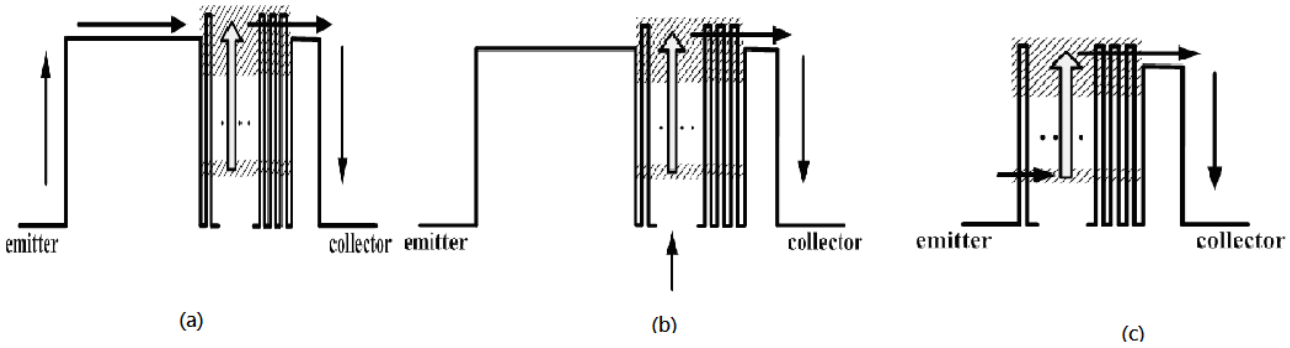

Figure 1. The schematic band diagram of (a) Detector 1, (b) Detector 2 and (c) Detector 3. The black arrows in these figures indicate the flows of electrons.

2. EXPERIMENTAL PROCEDURE

Two detectors are fabricated from the same sample but with different mesas. The epitaxy growth from bottom to top of this sample are an emitter layer, $Al_{0.28}Ga_{0.72}As$ thick barrier, a 15-period SL, $Al_{0.28}Ga_{0.72}As$ thin barrier and a collector layer. Each period of the SL is composed of 6.5 nm GaAs well and 3.5 nm $Al_{0.32}Ga_{0.68}As$ barrier (undoped). The absorption wavelength of the SL is from 6 to 10 μm.

To form bottom contact of detector 1, this sample is etched down to the emitter layer and evaporated metal (70 nm Ni/Ge/Au and 230 nm Au) onto the top of the collector and also onto the bottom as the emitter. Because the thick barrier may block the supply of electrons from the emitter, we fabricate another device for comparison. Detector 2 is etched down only to the SL active region and the emitter contact is directly fabricated on it. To further compare the performance and characters of

these two detectors, we fabricate 15-period-SL single-barrier Detector 3. Figure 1 (a), (b) and (c) show the band diagrams of Detector 1, 2 and 3. The black arrows in these figures indicate the flows of electrons.

The substrates of these three detectors are polished into 45° facet to skip normal-incidence issue and measure the photoresponse. The bias polarity is defined as positive if high potential is applied on the collector. Figure 2 shows the setup of the measurement of spectral response. Detectors are mounted on a cryostat system. Photocurrent of devices generated by the infrared source in FTIR is first amplified and converted to voltage signal by a low noise current preamplifier (Stanford Research SR570), and then input to the FTIR. The interference intensity is therefore transformed by the built-in program in FTIR to obtain the spectrum.

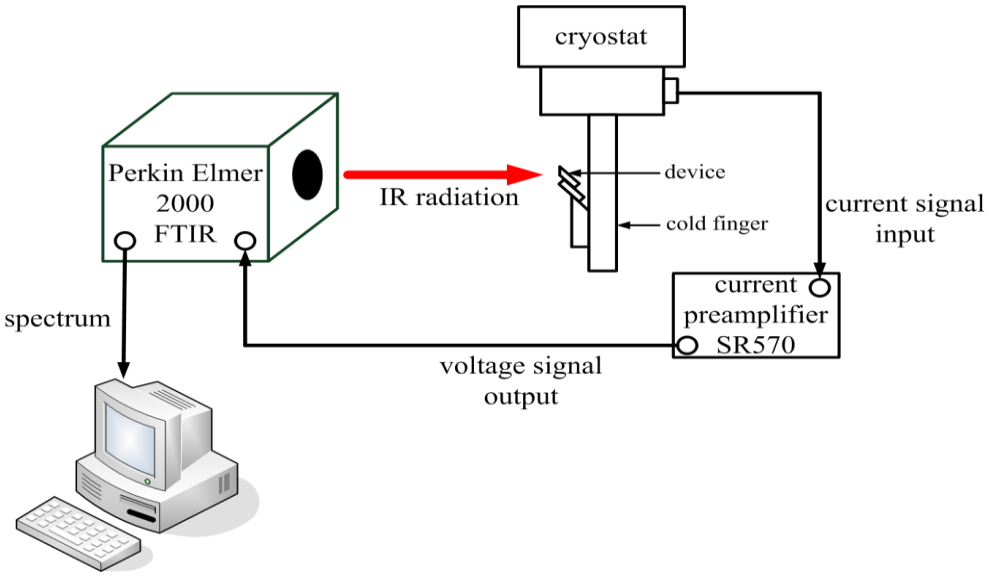

Figure 2. The schematic setup of the measurement of spectral response.

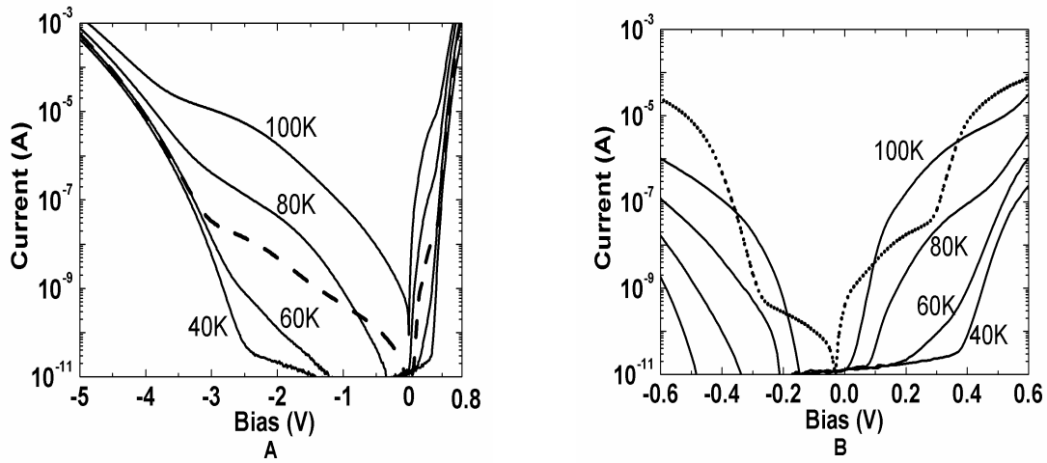

Figure 3. (a) The dark current (solid lines) at different temperatures and the photocurrent at 20 K (dashed line) versus the bias of Detector 1. (b) I-V curves of Detectors 2 at the same condition.

3. RESULTS AND DISCUSSION

In the following of this paper, we will present and compare these detectors' performances first, including current-voltage (*I-V*) characteristics, photoresponse and detectivity. Then, we will discuss the possible mechanisms which cause the differences between these detectors.

3.1. I-V Characteristics

I-V curves are measured at different temperature of Detector 1 (Figure 3 (a)) and 2 (Figure 3 (b)). Dark current at 40-100 K and 300 K background photocurrent measured at 20 K are shown in solid and dashed lines. A very asymmetric *I-V* relationship is observed in Detector 1. [8]

Clearly, Detector 2 shows higher 300 K background photocurrent and the lower dark current at any temperature. The dark current of Detector 2 at 80 K is lower than Detector 1 for an order at low bias, while the photocurrent is higher for more than one order at very low bias.

Many experimental *I-V* characteristics of quantum-well (QW) or quantum-dot (QD) detectors show the asymmetry with the applied bias [8-13]. The detail mechanism is not yet resolved completely. In Detector 1, although the sample structure is asymmetric, electrons have to traverse both barriers to generate the current no matter under positive or negative bias. Hence, the *I-V* curves are expected to be symmetric. The cause of the asymmetry will be discussed later.

3.2. Photoresponse

The spectral responsivity of these detectors is measured to further demonstrate the photocurrent improvement of Detector 2. The spectral responsivity versus wavelength at 80 K of Detector 1, 2 and 3, are shown in Figure 4. These spectra are measured under 0.15 V, 0.2 V and 0.25 V. The responsivity of Detector 1 is quite small. This is consistent with the resulted background photocurrent shown in Figure 3. We can also measure the response of Detector 1 (not shown here) under negative bias, but the applied bias has to be ten times larger than that under positive bias for the same magnitude of responsivity.

It is noted that Detector 2 has the higher responsivity than Detector 3 under all applied biases. In particular at very low bias such as 0.15 V, the responsivity at 9.2 μm of Detector 2 is 10 times higher than that at 9.4 μm of Detector 3. Even at the lower bias, the peak responsivity may be higher for more than one order. However, the responsivity difference between Detectors 2 and 3 is gradually decreased with increased bias.

In order to observe the responsivity trend with bias and temperature, Figure 5 (a) presents the spectral peak responsivity of Detector 1 and 2 at 9.2 μm, and Detector 3 at 9.4 μm versus the applied bias at 20 K (without squares) and 80 K (with squares) in linear scale, while Figure 5 (b) shows the same data but in log scale. In Figure5 (a), all the responsivity is increased with the applied bias and those of Detector 2 and 3 show less dependence on temperature than Detector 1. The threshold voltage

of Detector 2 is the lowest (0.03 V at 80 K or 0.06 V at 20 K), while that of Detector 1 is the highest. And in Figure 5 (b), Detector 2 shows the higher magnitude for at least one order than Detector 1 and 3 at very low bias. The enhanced photocurrent with temperature for Detector 1 is attributed to the less carrier depletion as temperature rises, while Detector 2 and 3 show no carrier depletion at all. This phenomenon will be discussed later. The causes of the lower threshold voltage and the dramatic increment of responsivity in Detector 2 will also be discussed together.

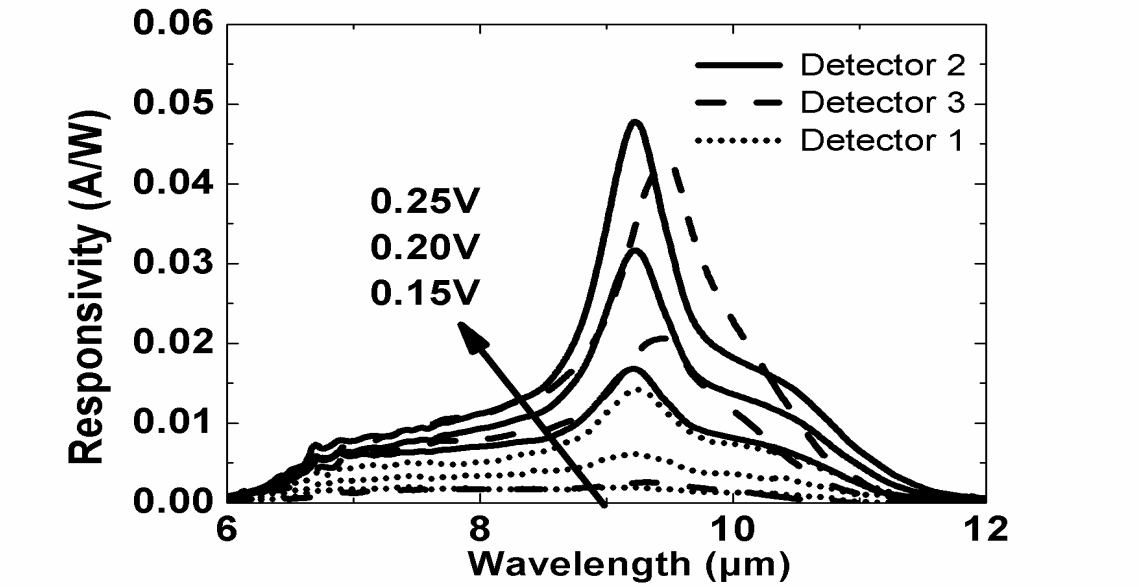

Figure 4. The spectral responsivity versus wavelength at 80 K of Detector 1 with dotted lines and Detector 2 with solid lines, Detector 3 with dashed lines at 0.15 V, 0.2 V and 0.25 V.

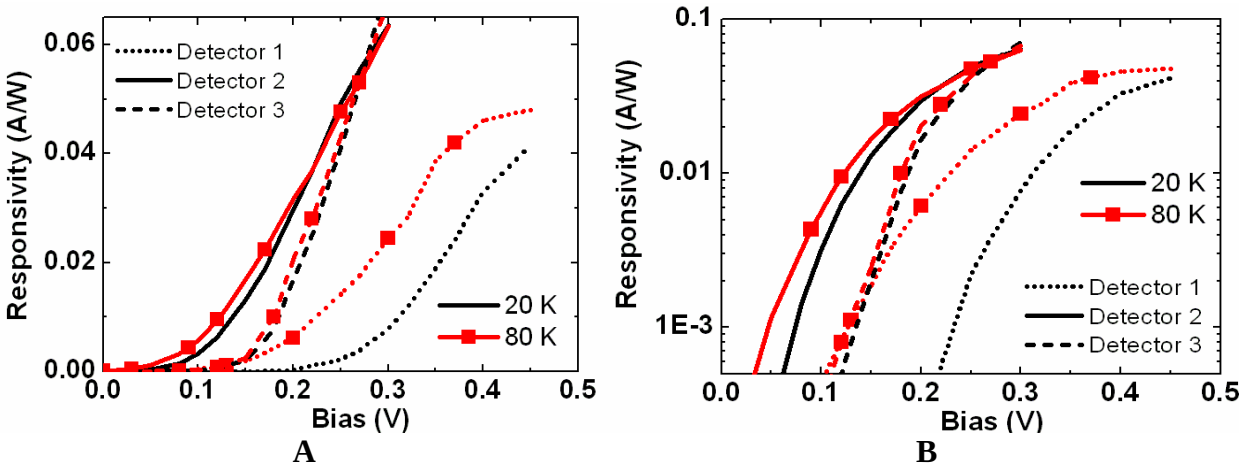

Figure 5. The peak responsivity comparison of Detector 1 (dotted lines), Detector 2 (solid lines) and Detector 3 (dashed lines) in (a) linear scale and (b) log scale. The lines with and without squares present the responsivity at 80 K and 20 K, respectively.

3.3. Detectivity

Due to the much higher responsivity than Detector 1 and 3 at very low bias, the detectivity of Detector 2 is also better. Table 1 shows the comparison of detectivity at 80 K and different wavelength of these three detectors and one of our previous QWIP samples whose structure is 50 periods of 6.1 nm GaAs well and 50 nm $Al_{0.23}Ga_{0.77}As$ barrier. It is demonstrated that Detector 2 at low bias has the highest detectivity among them. QWIP has much higher responsivity compared to Detector 2, but it has much higher dark current. So QWIP's performance is not the best of them. The maximum detectivity of Detector 2 is 1.2×10^{10} $cmHz^{1/2}/W$, which is the best among our previous works [10, 14-17]. So far, all experimental results show the photoresponse at low bias can be enhanced by inserted thick barrier. Next, we will discuss the possible mechanisms occurred in these devices.

Table. 1. The comparison of max detectivity, wavelength and associated bias at 80 K of Detector 1, 2, 3 and the QWIP.

	Wavelength(μm)	Bias (V)	Max Detectivity($cmHz^{1/2}/W$)
Detector 1	9.2	0.3	1.3×10^{9} $cmHz^{1/2}/W$
Detector 2	9.2	0.1	1.2×10^{10} $cmHz^{1/2}/W$
Detector 3	9.2	0.3	1.5×10^{9} $cmHz^{1/2}/W$
QWIP	10.5	4.0	2.0×10^{9} $cmHz^{1/2}/W$

3.4. Discussions

From Figure 3 (a) and (b), we can observe that the *I-V* relationship in Detector 1 is asymmetric, while that in Detector 2 is quite symmetric with respect to the bias. Because the only difference between these two devices is the position of emitter contact, we consider that the cause of the asymmetry is the limited supply of electrons from the emitter through the thick barrier under positive bias. Hence, it results in the electron depletion in the SL of Detector 1.

The band diagrams of Detector 1 under positive and negative bias are sketched in Figure 6 (a) and (b), respectively. Under positive bias, photo-generated and thermally excited electrons in the SL can go through the thin barrier easily to the collector. However, it is difficult to supply electrons from the emitter to the SL even though all the applied bias drops on the thick barrier. In this situation, the escaped electrons from the SL will go through the external circuit and accumulate at the interface between the emitter and the thick barrier. The left positive ions in the SL and the accumulated electrons will create a large electric field across the thick barrier to pull more electrons from the emitter. Due to the carrier depletion in the SL, no miniband will form and the responsivity will also be quite small, and the related results will be discussed in the following. Meanwhile, the large electric field makes the effective thickness of the thick barrier be almost negligible and electrons transport

through the two barriers with a high drift velocity and without being captured by the SL, which leads to the high dark current.

Moreover, the enhanced photocurrent with temperature of Detector 1 is because the scattering effect during the electron transport becomes more serious as temperature rises. As a result of it, more injection electrons are trapped in the SL to increase the photoresponse.

Besides, under negative bias as shown in Figure 6 (b), the electrons can be supplied from the collector easily.

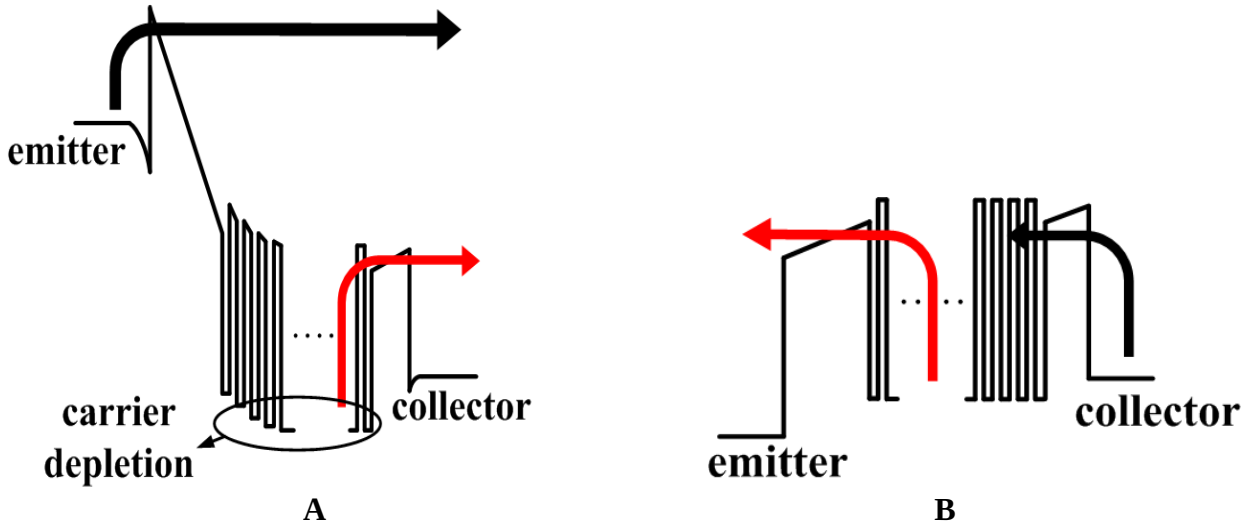

Figure 6. The band diagrams of Detector 1 under (a) positive and (b) negative bias

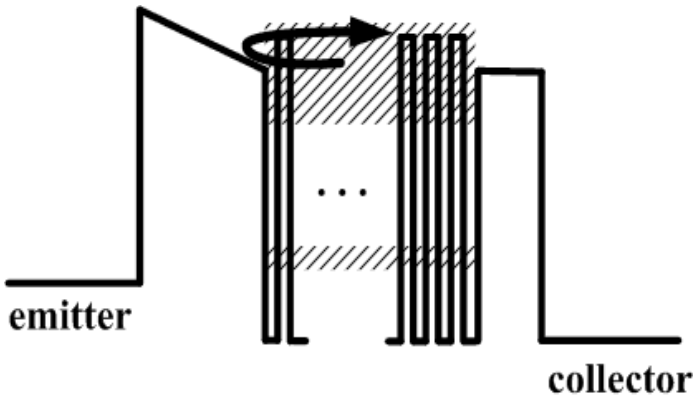

Figure 7. The band diagrams of Detector 2 under thermal equilibrium. The thick barrier is tilted to result in the electron oscillation in the second miniband.

If the injection current from collector is higher than the current flowing through the thick barrier, electrons accumulate in the SL and create a potential to block the supplied electrons and

balance the current. Therefore, no carrier depletion and accumulation will occur. And the current magnitude is thus determined by the thick barrier. This is why the applied bias under negative bias has to be higher than that under positive bias to have the same responsivity.

For Detector 2, the electrons escaped form the SL can be supplied from the metal contact immediately to overcome the carrier depletion problem and to improve the responsivity. Meanwhile, because the large electric field no longer exists, the dark current of Detector 2 is also lowered.

On the other hand, Detector 2 has the higher photocurrent than Detector 3 at low bias. In Detector 2, the emitter layer is left open and the thick barrier is tilted under thermal equilibrium as shown in Figure 7. Furthermore, the thin barrier in our design is 25 meV higher than the bottom state of the second miniband in the SL. It is more advantageous for the photoelectrons in the second miniband to oscillate and move back and forth between the two barriers especially at very low bias when the tunneling probability through the thin barrier is small. Because the responsivity of Detector 2 is about ten times higher than that of Detector 3 at around 0.1 V, we infer that the electrons in the SL of Detector 2 may bounce back and forth for more than ten times. This oscillation phenomenon enhances the transmission probability of the photoelectrons through the thin barrier and results in the higher responsivity and the lower threshold voltage in Detector 2.

As the applied bias rises, the tunneling probability through the thin barrier becomes so large that the oscillation phenomenon is less apparent and the responsivity difference of the two detectors is gradually decreased. Due to no miniband originated from the carrier depletion in Detector 1 and no thick barrier for electron oscillation in Detector 3, Detector 2 has the better performance at the very low bias and is more suitable for low-power applications.

4. CONCLUSION

In conclusion, we have studied SLIP whose structure is a 15-period SL sandwiched between two rear and front barriers. In this detector, the photoelectrons excited from first miniband to second miniband of the SL can oscillate in the bottom of second miniband between front and rear barriers to improve performance at very low bias. Because of the limited supply of the electrons from the emitter to the SL cause the carrier depletion inside the SL. A large electric field across the thick barrier worsens the performance of the detector. The metal contact is formed on the SL layer instead of the emitter layer to solve this problem. The new-processed detector shows much higher responsivity at very low bias because the photoelectrons oscillation between the two barriers. This new-processed detector also shows the higher detectivity than the single-barrier SLIP and QWIP presented in our previous papers. This new-processed SLIP is potential for the low-power consumption applications due to best performance at low bias.

ACKNOWLEDGEMENT

This work was supported by National Science Council of Taiwan, under Contract NSC 100-2221-E-390-017 and NSC 97-2221-E-002-053-MY3.

References

1. S. Ozer, O. O. Cellek and C. Besikci," *Infra. Phys. & Technol*. 47 (2005) 115
2. E. Costard, Ph. Bois, X. Marcadet and A. Nedelcu, *Infra. Phys. & Technol.* 47 (2005) 115.
3. S. D. Gunapala, S. V. Bandara, J. K. Liu, C. J. Hill, S. B. Rafol, and J. M. Mumolo," *IEEE Trans. Electron. Dev.* 50 (2003) 2353
4. B. F. Levine, "Quantum-well infrared photodetector," *J. Appl. Phys.* 74 (1993) 1
5. H. Schneider, T. Maier, J. Fleissner, M. Walther, P. Koidl, G. Weimann, W. Cabanski, M. Finck, P. Menger, W. Rode, and J. Ziegler, *Infra. Phys. & Technol.* 47 (2005) 53
6. C. C. Chen, H. C. Chen, M. C. Hsu, W. H. Hsieh, C. H. Kuan, S. Y. Wang and C. P. Lee *J. Appl. Phys.* 91 (2003) 943
7. C. C. Chen, H. C. Chen, C. H. Kuan, S. D. Lin and C. P. Lee, *Appl. Phys. Lett.* 80, (2002) 2251
8. S. H. Lin, J. Y. Feng, J.H. Lu, T. S. Lay, C. H. Kuan , *J. Electrochemical Soc*.158 (2011) H370
9. C. S. Wu, C. P. Wen, P. Reiner, C. W. Tu and H. Q. Hou, *Solid State Electron*. 39 (1996) 1253
10. S. H. Lin, Y. H. Wang, C. W. Chang, J. H. Lu, C. C. Chen, and C. H. Kuan, *Cutting Edge Nanotechnology*, p. 121, In-Tech, Croatia (2010).
11. S. F. Tang, S. Y. Lin and S. C. Lee, *IEEE Trans. Electron Dev.* 49 (2002) 1341
12. J. Jiang, K. Mi, W. Zhang, H. Lim, T. O'Sulliwan, T. Sills, M. Razeghi, G. J. Brown and M. Z. Tidrow, *Appl. Phys. Lett*. 84 (2004) 2232
13. H. C. Liu, R. Wasilewski, M. Buchanan and H. Chu, *Appl. Phys. Lett* 63 (1993) 761
14. M. C. Hsu, Y. F. Hsu, S. Y. Lin and C. H. Kuan, *IEEE Trans. Electron Dev.* 47 (2000) 944
15. J. H. Lu, Y. Y. Yang, C. C. Chen, C. H. Kuan, H. D. Chen and S. C. Lee, *Infra. Phys. & Technol.*44 (2003) 399
16. J. H. Lu, K. J. Wu, K. J. Hsieh, C. H. Kuan, C. W. Yang, S. L. Tu, J. Y. Feng and T. S. Lay, *IEEE J. Quant. Electron* 43 (2007) 72
17. J. H. Lu, Y. C. Wang, C. L. Wang, C. H. Kuan, C. W. Yang, S. L. Tu, J. Y. Feng,and T. S. Lay, *J. Appl. Phys.* 102 (2007) 074542